Journal of Marine Science and Technology

Volume 24 | Issue 3 Article 7

PREDICTIONS OF STRESS-STRAIN CURVE AND FATIGUE LIFE FOR AISI 316 STAINLESS STEEL IN CYCLIC STRAINING

Liang-Hsiung Chou
Department of Civil and Water Resources Engineering, National Chiayi University, Chiayi, Taiwan, R.O.C

Yung-Chuan Chiou
Department of Biomechatronic Engineering, National Chiayi University, Chiayi, Taiwan, R.O.C., solas@mail.ncyu.edu.tw

Chia-Chin Wu
SuperAlloy Industrial Co. Ltd, Dou-Liu, Taiwan, R.O.C

Ying- Jen Huang
Department of Biomechatronic Engineering, National Chiayi University, Chiayi, Taiwan, R.O.C.

Recommended Citation

Chou, Liang-Hsiung; Chiou, Yung-Chuan; Wu, Chia-Chin; and Huang, Ying- Jen (2016) "PREDICTIONS OF STRESS-STRAIN CURVE AND FATIGUE LIFE FOR AISI 316 STAINLESS STEEL IN CYCLIC STRAINING," *Journal of Marine Science and Technology*: Vol. 24: Iss. 3, Article 7.
DOI: 10.6119/JMST-015-0820-1
Available at: https://jmstt.ntou.edu.tw/journal/vol24/iss3/7

Journal of Marine Science and Technology, Vol. 24, No. 3, pp. 426-433 (2016)
DOI: 10.6119/JMST-015-0820-1

PREDICTIONS OF STRESS-STRAIN CURVE AND FATIGUE LIFE FOR AISI 316 STAINLESS STEEL IN CYCLIC STRAINING

Liang-Hsiung Chou[1], Yung-Chuan Chiou[2],
Chia-Chin Wu[3], and Ying- Jen Huang[2]

Key words: 316 stainless steel, cyclic behavior, stress-strain response simulation, life predictions.

ABSTRACT

In this study, experimental observations have been performed to understand the cyclic stress-amplitude response, the cyclic hardening/softening characteristics and the cyclic fatigue properties of AISI 316 stainless steel. Based on the experimental observations, these results are found so that the tested AISI 316 stainless steel possesses cyclic hardening characteristics. The shape of the stable hysteresis loop is symmetrical in tension and compression. The Massing cyclic stress-strain behavior is obviously absent. For the case of the absence of the Massing behavior, the power-law type equation is successfully applied to simulate the shape of the stable hysteresis loop at all applied levels of fully-reversed cyclic straining. For the ε_a-based and $\sigma_{\max}\varepsilon_a$-based fatigue life curves, the typical expressions are developed via cyclic fatigue properties. Besides, a power-law type relationship is also used to develop the fatigue life curve. In contrast to the typical expression, it is found that the power-law relationship is a viable and valid expression in fatigue life predictions. Similarly, the power-law relationship is also used to describe the correlation between the cumulative plastic strain energy W_f with the corresponding the fatigue life cycle N_f. Based on the comparison between the predicted and experiment cycles, it is confirmed that the predicted value of W_f calculated on the basis of the simulated hysteresis loop is capable of yielding reasonable life predictions via the W_f - N_f curve.

Paper submitted 05/10/15; revised 06/30/15; accepted 08/20/15. Author for correspondence: Yung-Chuan Chiou (e-mail: solas@mail.ncyu.edu.tw).
[1] Department of Civil and Water Resources Engineering, National Chiayi University, Chiayi, Taiwan, R.O.C.
[2] Department of Biomechatronic Engineering, National Chiayi University, Chiayi, Taiwan, R.O.C.
[3] SuperAlloy Industrial Co. Ltd, Dou-Liu, Taiwan, R.O.C.

I. INTRODUCTION

Generally, components and structures in service are often subjected to cyclically varying loading such as vibratory loading, earthquake loading and fatigue. Therefore, observation and analysis of stress-strain responses in cyclic loading conditions is a basic step for designers. Generally, for most metals in cyclic loading, it is found that the variation of cyclic stress-strain response is violent and rapid during the early stages of cycling and then does not vary appreciably for the majority of the fatigue life. Based on this observation, the hysteresis loop from near half the fatigue life is usually used to represent the stable stress-strain behavior in design. Generally, in order to assess the durability of component subjected to cyclic loading, the named cyclic stress-strain curve by relating the stable stresses amplitude σ_a to the controlled strain amplitude ε_a is usually developed. In the regime of elastic-plastic deformation, the response of a material during a cyclic straining is in the form of a closed hysteresis loop and the area within the closed loop represents the plastic energy density ΔW_p. Moreover, while the hysteresis loop curves in tension at various strain amplitude have the same shape, the behavior is named the Massing cyclic stress-strain behavior (Halford, 1966). In contrast to the cyclic stress-strain curve, the curve by expanding the cyclic stress-strain curve with a scale factor of two is named the Massing curve. And, while the Massing cyclic stress-strain behavior reveals in material, the named Massing curve can be employed to simulate the shape of stable hysteresis loop and the corresponding value of ΔW_p is obtained. However, the Massing cyclic stress-strain behavior is seldom occurred in many engineering metals. Hence, a need exists to formulate the relationships on the shape of hysteresis loop of a material without the Massing cyclic stress-strain behavior. It is agreeable that the irreversible cumulative plastic strain energy, $W_f = \Delta W_p \times N_f$, would lead to fatigue failure. Therefore, in predicting accumulated plastic strain energy, it is valuable to establish a simple and accurate approach on the simulation of the shape of hysteresis loop.

For a simulation on the shape of the stress-strain hysteresis

loop, many experimental models (Prager, 1956; Mroz, 1967; Garud, 1981; Bower, 1989) and cyclic plasticity models (Morrow, 1965; Valanis, 1980; Lefebvre and Ellyin, 1984; Chaboche, 1991; Wittke and Rie, 1998; Kwofie, 2003) have proposed. In life prediction method, strain-based life curve expressed by cyclic fatigue properties is commonly used to predict the cycles of fatigue life. Conventionally, the required cyclic fatigue properties are obtained from performing a series of completely reversed symmetrical cyclic straining tests. However, components are seldom subjected to a symmetrical cyclic straining. Consequently, in considering mean stress/strain effects on the fatigue life, the damage parameter obtained from the fully reversed fatigue tests needs to be modified or developed. Consequently, the damage parameter $\sigma_{\max}\varepsilon_a$ is proposed (Smith et al., 1970) and then the $\sigma_{\max}\varepsilon_a$-based life relationship is expressed as a function of the fatigue life, N_f, via fatigue properties.

Generally, performing a fatigue life prediction, numerical calculations are often inevitable by using strain-based and $\sigma_{\max}\varepsilon_a$-based life curves expressed in fatigue properties. Therefore, for strain-based and $\sigma_{\max}\varepsilon_a$-based life curves, a simple and viable expression is required. Besides, in considering the load path effect on fatigue life, energy-based life curve is commonly used in the prediction of the cycles to failure. It is well known that AISI 316 stainless steel is widely used as a component of pressure vessels and piping systems in the petrochemical and nuclear industries due to its high ductility and good resistance to corrosion. Therefore, the deformation response of AISI 316 stainless steel subjected to cyclic strain-controlled and stress-controlled loading has been extensively studied (Polak et al., 1996; Abduluyahed and Kurzydlowski, 1998; Tokaji et al., 2004; Wang et al., 2005; Paiva and Barbosa, 2008; Kamaya, 2010; Bacon et al., 2013). The object of this study is to observe and analyze the material response of the AISI 316 stainless steel in cyclic straining. Simultaneously, the cyclic stress-strain curve, strain-based and $\sigma_{\max}\varepsilon_a$-based life curves expressed by cyclic fatigue properties are developed. For the case without the Massing behavior, the stress-strain relationship based on the Ramberg-Osgood type equation is developed to simulate the shape of hysteresis loop curve. Moreover, for the strain-based and the $\sigma_{\max}\varepsilon_a$-based life curves, a direct power-law relationship is developed in order to avoid the cumbersome procedure of estimating the fatigue cycle. The comparison in the predictions of fatigue life is performed in order to realize whether the power-law relationship is a suitable expression. Moreover, the fatigue life curve based the damage parameter W_f is also developed via a power-low form in this study. For all developed life-curves, life prediction capabilities are respectively examined in this study.

II. EXPERIMENTAL PROCEDURES

1. Material and Specimen

The AISI type 316 stainless steel was used for the experiments. The chemical composition of the tested material is given in Table 1. The tested materials in as-received condition are machined from round bars by CNC lathe to produce the specimen with a cylindrical shape as shown in Fig. 1. However, for the fatigue specimen, a smooth surface in the gauge section is required. Therefore, after machining, a fine emery paper is used to remove all circumferential scratches and machine marks on the surfaces of the fatigue specimens in this experiment.

Table 1. Chemical compositions of AISI 316 stainless steels (weight%).

C	Si	Mn	P	S	Ni	Cr	Cu	Fe
0.054	0.45	1.48	0.022	0.023	10.26	16.74	2.18	bal.

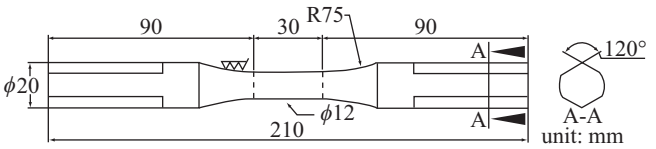

Fig. 1. Shape and dimensions of test specimen for AISI 316 stainless steel.

2. Mechanical Testing

For the AISI type 316 stainless steels, in order to understand the stress-strain response in tension, the basic fatigue properties and the cyclic response characteristics, the tensile test and the fatigue life test were performed in this study. In the tensile test, the tested specimens were uniformly loaded at a crosshead rate of 0.01 mm/sec. In the fatigue life test, the specimens were cycled using tension-compression loading under total strain control. Eight levels of controlled strain amplitude were considered for the determinations of the basic fatigue properties and strain-life curve in this study. For all fatigue life tests, the waveform with a triangular strain-time was carried out at the frequency of 0.5 Hz and the longitudinal strains were continuously measured using a longitudinal extensometer with a 25 mm edge separation. The Max software, integrated in the testing system, was used to simultaneously sample 400-500 experimental points around the hysteresis loop in every cycle throughout the fatigue life test. Testing was performed until the specimen failed in the fatigue life test. The number of cycles to failure, N_f, was defined as the number of cycles performed before the recorded peak tensile stress dropped to a value of approximately 10% below the plateau stress on the cyclic-stress-response curve. Near half-life hysteresis loop data were defined as the stable response of the tested material for cycling loading and were used to determine the cyclic fatigue properties in this study. All mechanical tests were performed on a closed-loop servo-hydraulic test machine.

III. EXPERIMENTAL RESULTS AND OBSERVATION

1. Monotonic and Cyclic Deformation Behavior

In this study, firstly, monotonic and cyclic deformation

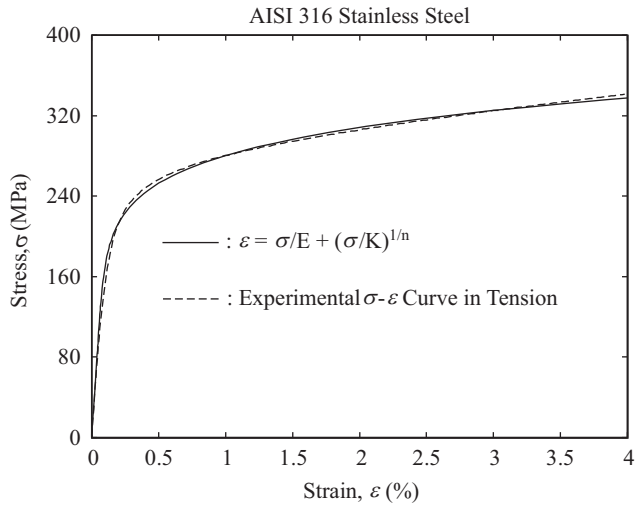

Fig. 2. Comparison of experimental and simulation results for the monotonic stress-strain curves.

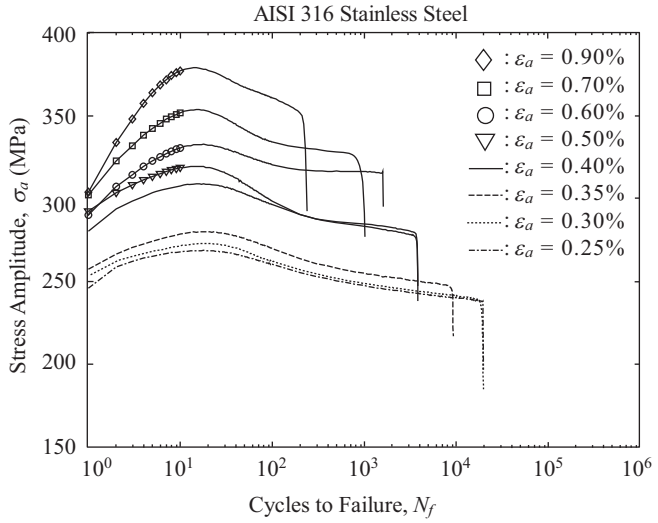

Fig. 3. Cyclic stress response curves for AISI 316 stainless steel.

behaviors of the AISI 316 stainless steel subjected to the monotonic loading and cyclic straining are observed and analyzed, respectively. Generally, for the strain shown in Fig. 2, it is separated into elastic strain, ε_e, and plastic strain, ε_p. And, elastic and plastic strains can be directly calculated from $\varepsilon_e = \sigma/E$ and $\varepsilon_p = \varepsilon - \varepsilon_e$. E is elastic modulus. Additionally, for most metals, the power-law type equation is commonly used to correlate stress with plastic strain and relationship is expressed as

$$\sigma = K(\varepsilon_p)^n \tag{1}$$

In Eq. (1), the fitting constant K is called the strength coefficient and the value of n is called the strain-hardening exponent. Furthermore, the strain can be stated as a function of stress using Eq. (1) and is described by

$$\varepsilon = \sigma / E + (\sigma / K)^{1/n} \tag{2}$$

Table 2. AISI 316 stainless steel cyclic fatigue properties.

E	K'	n'	σ'_f	b	ε'_f	c
MPa	MPa		MPa			
202335	899.08	0.1901	663.25	-0.0903	0.1895	-0.4657

The relationship represented as Eq. (2) is referred to as Ramberg-Osgood type equation. In Eq. (1), values of K and n were obtained via performing a least squares fit of stress, σ, versus plastic strain, ε_p, data in log-log scale. In this study, the value for K is 506.97 and for n is 0.1247. As shown in Fig. 2, obviously, the simulated curve based on Eq. (2) provides a good agreement with experimental data. Fig. 3 presents stress amplitudes versus number of cycles to failure plots of AISI 316 stainless steel subjected to fully reversed cycle straining at eight various strain amplitudes. For each recorded cyclic stress curve shown in Fig. 3, it is found that the variation of the measured stress amplitude per cycle with cycle presents a rapid increase at initially about ten cycles, and then the measured stress amplitude per cycle gradually decreases prior to failure. Based on the above observation in the Fig. 3, values from a hysteresis loop recorded near half of the cycles to failure are used as being representative of the approximately stable behavior in this study.

2. Stable Stress-Strain Response and Fatigue Properties

Essentially, for many engineering metals, the Ramberg-Osgood type equation is capable of yielding highly accurate correlation between stable stress amplitude and strain amplitude. Therefore, the expression which is analogous to Eq. (2) is also applied to develop the cyclic stress-strain curve in this study and is expressed as:

$$\varepsilon_a = \frac{\sigma_a}{E} + \left(\frac{\sigma_a}{K'}\right)^{1/n'} \tag{3}$$

In Eq. (3), K' is called the cyclic strength coefficient and n' is cyclic strength coefficient. Similarly, both parameters of K' and n' could be determined by the least-squares technique and presented in Table 2. As shown in Fig. 4, a good agreement exists between the solid line of simulation by Eq. (3) and those measured data from the stable hysteresis loops. Moreover, it is found in this figure that cyclic stress-strain is above the monotonic tension curve. The observation indicates that the tested AISI 316 stainless steel is a cyclic hardening material. Generally, experimental stable hysteresis loops were plotted with shifted axes such that their compressive loops all fall at the same origin. The link curve of the tips of experimental stable hysteresis loops plotted in a common stress-strain diagram is called the Massing curve.

According the definition on the Massing curve, the curve can be obtained by doubling the cyclic stress-strain curve and the equation of the Massing curve can be formulated as

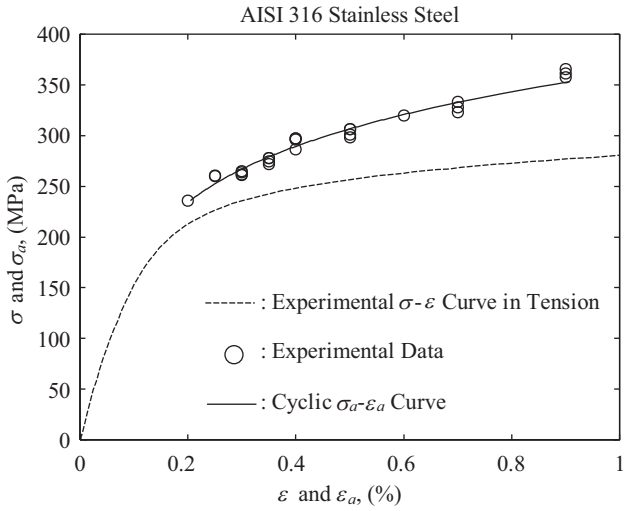

Fig. 4. Comparison of the monotonic and cyclic stress-strain curves.

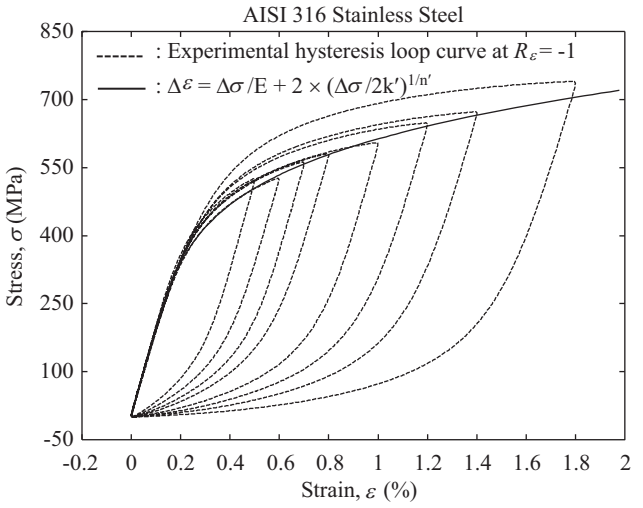

Fig. 5. Comparison of experimental stable hysteresis loops and the solid curve from expanding cyclic stress-strain curve with a scala factor of two.

$$\Delta\varepsilon = \frac{\Delta\sigma}{E} + 2\times\left(\frac{\Delta\sigma}{2K'}\right)^{1/n'} \tag{4}$$

Generally, when stable hysteresis loops plotted in a common stress-strain diagram and loading curves for all of the used hysteresis loops fall on the corresponding Massing curve, the specific stress-strain behavior is named as Massing cyclic stress-strain behavior. Obviously, when a material exhibits the Massing cyclic stress-strain behavior at all of the considered strain amplitudes, Eq. (4) can be applied to simulate the stable hysteresis loop curve in tension. Furthermore, the simulation on the shape of the stable hysteresis loop can be completed for a material that exhibits symmetric behavior in tension and compression. For this case, by integrating the area within the simulated loop, the stable plastic strain energy density, ΔW_p, can be predicted. As shown in Fig. 5, the comparison between the Massing curve and eight actual hysteresis loops simultaneously plotted in relation coordinates was also carried out to determine whether the tested AISI 316 stainless steel possess Massing cyclic stress-strain behavior. It is found that the Massing curve correspond not well with all hysteresis loops in tension. The observation indicates the Massing cyclic stress-strain behavior was not exhibited in the tested AISI 316 stainless steel. In other words, Eq. (4) could not provide an accurate simulation on the hysteresis loop curve in tension in the strain ranges from 0.50 % to 1.80 %.

In determination of fatigue properties, the plastic and elastic amplitudes (ε_a^p and ε_a^e) of hysteresis loops at half fatigue life are respectively plotted versus the number of reversals to failure, $2N_f$, on a log-log scale and are linearized. For the correlation between ε_a^e and $2N_f$, the corresponding equation is given by

$$\varepsilon_a^p = \varepsilon'(2N_f)^c \tag{5}$$

The relationship is often called the Coffin-Mason equation. And, for the $\varepsilon_a^e - 2N_f$ curve, the relationship which is often named the Basquin equation is given by

$$\varepsilon_a^e = \frac{\sigma_f'}{E}(2N_f)^b \tag{6}$$

Since the total strain amplitude is the sum of the plastic and elastic amplitudes, the relationship between total strain amplitude and the number of reversals to failure can be rearranged as

$$\varepsilon_a = \frac{\sigma_f'}{E}(2N_f)^b + \varepsilon_f'(2N_f)^c \tag{7}$$

According to the Eqs. (5) and (6) and the fatigue data of AISI 316 stainless steel, by performing a least-square fit on log-log plots of ε_a^p versus $2N_f$ and ε_a^e versus $2N_f$, then, the four constants, N'_f, c, σ'_f and b are evaluated and are present in Table 2. Fig. 6 shows a superimposed plot of elastic, plastic and strain-life curves as the basis of the fatigue data. As shown in Fig. 6, it is clear that those fitted curves have good correlations with the experimental results. It is noted that the plotted data values in Fig. 6 are obtained by performing a mean value calculation on the results under the same experimental conditions.

V. DISCUSSIONS

1. Model of Stable Hysteresis Loop Curve via the Ramberg-Osgood Type Equation

As shown in Fig. 5, Massing cyclic stress-strain behavior was absent in the stable stress-strain response of the tested material. Consequently, the named Massing curve obtained from

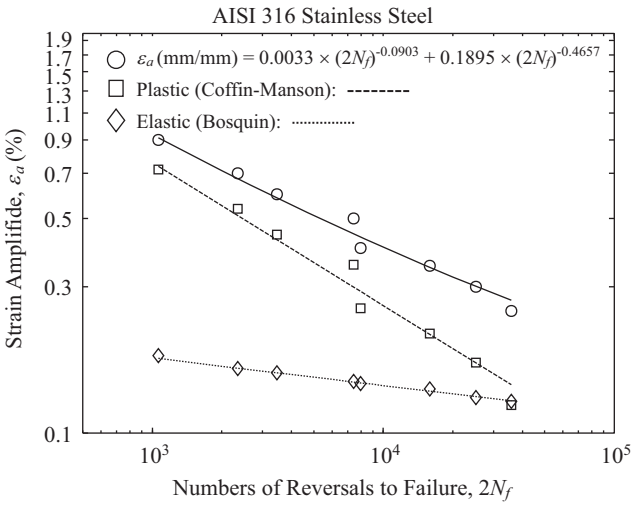

Fig. 6. Elastic, plastic and total strain versus reversals curves for AISI 316 stainless steel.

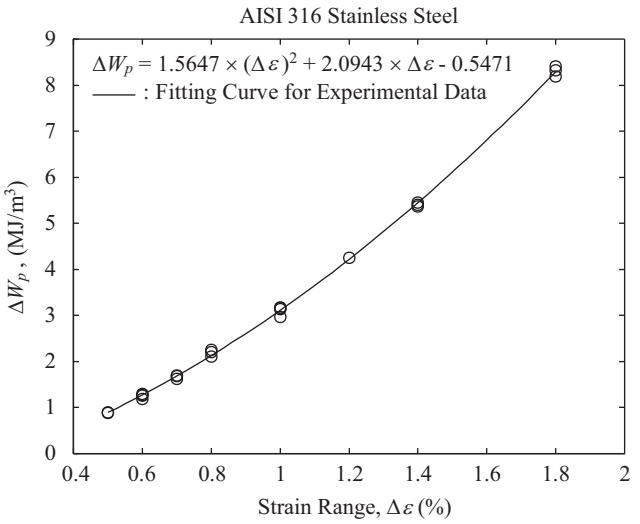

Fig. 7. Compasion of the fitting curve and the experimental plastic energy density data for AISI 316 stainless steel.

the expanded cyclic stress-strain curve could not provide an accurate description on the hysteresis loop curve in tension shown in Fig. 5. However, considering the fatigue fracture mechanics and the life assessment, a reasonable accuracy description on the shape of stable hysteresis loop is important to evaluate the stable plastic strain energy density ΔW_p. For the tested material without the Massing behavior, in this study the Ramberg-Osgood type equation is employed to describe the shape of hysteresis loop curve since the type equation has the characteristic that provides a single smooth curve for stress-strain response in metal. Similar to Eq. (2), the correlation of the stress and strain corresponding to any point on the stable hysteresis loop curve in tension is expressed as:

$$\varepsilon = \frac{\sigma}{E} + \left(\frac{\sigma}{H}\right)^{1/\beta} \tag{8}$$

Apparently, in Eq. (8), the term $\left(\frac{\sigma}{H}\right)^{1/\beta}$ presents the plastic strain and E is the modulus of elasticity. In essence, both parameters H and β must be obtained while Eq. (8) is employed to perform a simulation on the stable hysteresis loop curve in tension. In terms of the determination of both parameters H and β, both symbols σ_H and ε_{Hip} present the stress and plastic strain located on the tips of the stable hysteresis loop in a common stress-strain diagram. Essentially, corresponding to a controlled strain range $\Delta\varepsilon$, the magnitudes of σ_H and ε_{Hip} are respectively equal to the values of $\Delta\sigma$ and $\Delta\varepsilon_p$ and are also determined via the Massing curve. It is known that the area within the stable hysteresis loop represents the plastic strain energy density ΔW_p when stable. Additionally, for a material that exhibits symmetric in tension and compression, the stable plastic strain energy density corresponding to the specified strain range $\Delta\varepsilon$ is calculated via Eq. (8) and the parameter β can be related by:

$$\Delta W_p = \oint \sigma \times (d\varepsilon_e + d\varepsilon_p) = \frac{1-\beta}{1+\beta}\sigma_H \varepsilon_{Hip} \tag{9}$$

Apparently, the specific parameter β is also determined once those values of ΔW_p, σ_H(= $\Delta\sigma$) and ε_{Hip}(= $\Delta\varepsilon_p$) are given. For the parameter H, it is rewritten as

$$H = \frac{\sigma_H}{(\varepsilon_{Hip})^\beta} = \frac{\Delta\sigma}{(\Delta\varepsilon_p)^\beta} \tag{10}$$

According Eq. (10), the parameter H is obtained while those values of σ_H, ε_{Hip} and β are known. In contrast to the procedures in determination of parameters used in the monotonic and cyclic stress-strain curves, it is obvious that the procedure in Eq. (8) is different. According the above discussion, both parameters H and β in Eq. (8) can be determined from the value of ΔW_p and the Massing curve known for a material with symmetric behavior in tension and compression. Once both parameters H and β have been determined, Eq. (8) can be employed to calculate the values of strain and stress corresponding to any point on the stable hysteresis curve in tension. Simultaneously, the data from Eq. (8) is used to generate the stable hysteresis curve in compression. Under this condition, the stable hysteresis loop can be further constructed. Here, based on the observation in Fig. 5, it is accepted that the stable hysteresis loops are symmetrical with respect to tension and compression in the strain ranges from 0.50 % to 1.80 %. Moreover, in order to perform a series of simulation on the stable hysteresis curve in tension in the whole range of strain amplitudes tested, it is necessary to develop the correlation between ΔW_p and $\Delta\varepsilon$. In the form of ΔW_p - $\Delta\varepsilon$ relationship, an expression of algebraic form is set up to describe the correlation in the strain range from 0.50 % to 1.80 %. As shown in Fig. 7, the correlation seems appropriate to represent the vari-

Table 3. Summary of the calculated results for H and β.

$\Delta\varepsilon$	0.50	0.60	0.70	0.80	1.00	1.20	1.40	1.80
β	0.173	0.170	0.168	0.166	0.158	0.146	0.133	0.105
H	1427	1408	1400	1386	1341	1281	1218	1099

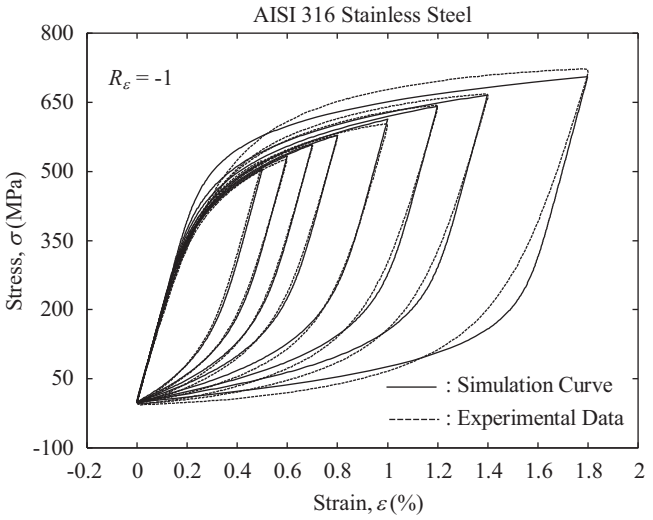

Fig. 8. Comparison of the experimental and simulated the hysteresis loop curves.

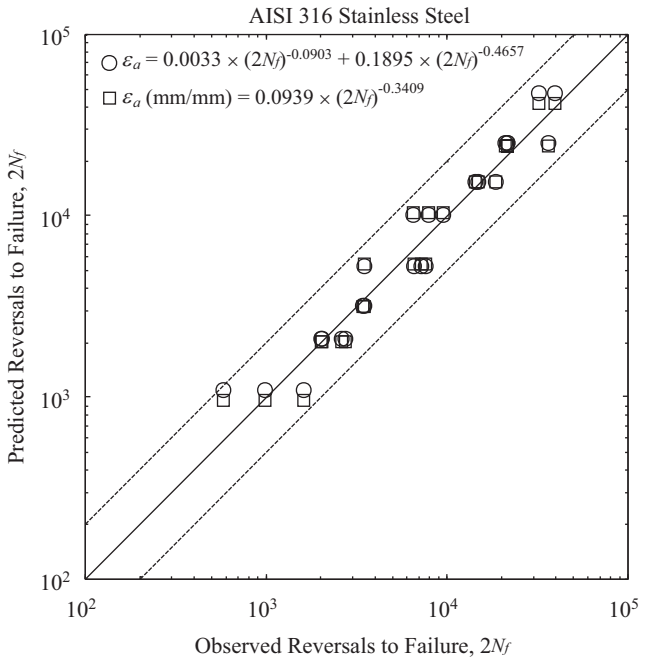

Fig. 9. Fatigue life predictions based on the strain-life curves of AISI 316 stainless steel.

ation of ΔW_p with $\Delta\varepsilon$ in the form of a quadratic Equation. According to the above discussion, for a specified value of $\Delta\varepsilon$, the empirical relations between ΔW_p and $\Delta\varepsilon$ shown in Fig. 7 and the Massing curve are used to calculate the corresponding values of H and β via Eq. (9) and Eq. (10). Table 3 summarizes the calculated results via the Massing curve and the relationships presented on Fig. 7 at each of the specified strain range. By using Eq. (8) and Table 3, the stress and strain corresponding to any point on the stable hysteresis loop curve in tension presented in Fig. 5 is calculated. As expected, the shape of the stable hysteresis loop at each of the eight strain amplitudes considered in this study is completed by the data generated from Eq. (8). Fig. 8 presents a comparison between the experimental and simulation results. It can be seen that experimentally measured data and the fitted curve based on Eq. (8) are in close agreement in Fig. 8.

2. Fatigue Life Predictions

In contrast to the Basquin-Coffin-Manson relationship, a direct power-law relationship between ε_a and $2N_f$ is commonly used to describe the strain-life curve since it provides a simple calculation on the determination of the number of reversals to failure. In a manner analogous to Eq. (5) and Eq. (6), by using the log-log linear regression analysis of the applied strain amplitude ε_a with respect to the corresponding reversals to failure $2N_f$, the values of constant and exponent used in the power-law relationship are 0.0939 and -0.3409. In this study, the experimental reversal $2N_f$ was compared with the reversal calculated according to both the relationships presented in Fig. 9. As shown in Fig. 9, it can be seen that all of the data points fall within a factor of two scatter bands and it is found that the power-law relationship gave better predictions than the Basquin-Coffin-Manson relationship. Consequently, the power-law relationship is a viable and valid expression for the strain-life curve of the tested AISI 316 stainless steel. For the damage parameter $\sigma_{\max}\varepsilon_a$, the fatigue curve is expressed by fatigue constants as

$$\varepsilon_a \varepsilon_{\max} = \frac{(\sigma_f')^2}{E}(2N_f)^{2b} + \sigma_f'\varepsilon_f'(2N_f)^{b+c} \qquad (11)$$

Essentially, the magnitude of max stress $\sigma_{\max}$ shown in Eq. (11) is equal to the value of stress amplitude σ_a for a material subjected completely reversed cyclic straining. Apparently, for Eq. (11) presented in Fig. 10, it is inevitable to perform a numerical operation in the prediction of the number of reversals to failure. Similarly, the $\varepsilon_a\sigma_{\max}$-based life curve, expressed as a power law function, has also developed in avoiding the cumbersome procedure of estimating the reversals to failure. The required constant and exponent are determined via a least-square fit on the log-log plots of the measured $\sigma_{\max}\varepsilon_a$ against $2N_f$ and are also presented in Fig. 10. Using both life curves presented in Fig. 10, the predictions of the number of reversals to failure have been performed and the comparison between the experimental data and the predicted value has also shown in Fig. 10. It can be seen that the predicted results are in good agreement with the experimental data and there is not a significant difference in making reversal prediction. Besides both ε_a and $\sigma_{\max}\varepsilon_a$ damage parameters, the

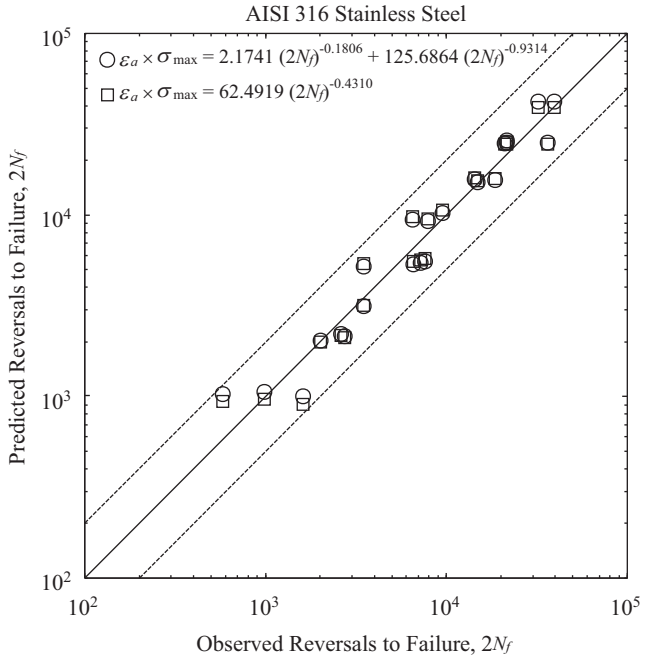

Fig. 10. Fatigue life predictions based on the $\sigma_{max}\varepsilon_a$-life curves of AISI 316 stainless steel.

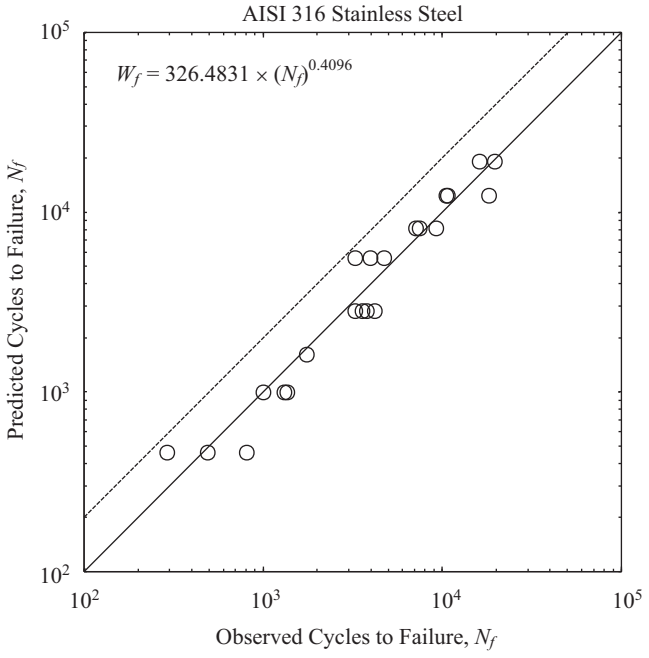

Fig. 11. Fatigue life predictions based on the W_f - N_f curve of AISI 316 stainless steel.

cumulative plastic strain energy approach is usually used to perform the fatigue prediction in low cycle fatigue regimes. However, for cyclic loading, the cyclic stress-strain response of metals is often drastically altered in early fatigue cycles and then remains almost constant for the majority of the fatigue life. Therefore, in applying the total plastic strain energy W_f to perform fatigue life prediction, the magnitude of W_f is essential considered as the product of ΔW_p and N_f. Similarly, in this study, the relationship between W_f and N_f is expressed as a power-low relationship and is found to be

Table 4. Summary of the calculated results for Ω.

Life curve	Ω
$\varepsilon_a = 0.0033 \times (2N_f)^{-0.0933} + 0.1895 \times (2N_f)^{-0.4857}$	0.3072
$\varepsilon_a = 0.0714 \times (N_f)^{-0.3408}$	0.2860
$\varepsilon_a\sigma_{max} = 2.1741 \times (2N_f)^{-0.3808} + 125.6864 \times (2N_f)^{-0.9224}$	0.2820
$\varepsilon_a\sigma_{max} = 46.3532 \times (N_f)^{-0.4320}$	0.2717
$W_f = 326.4831 \times (N_f)^{0.4098}$	0.2929

$$W_f = 326.4831 \times (N_f)^{0.4096} \tag{12}$$

In this study, on the basis of the simulated hysteresis loop, the value of W_f is calculated and then the corresponding predicted fatigue life is determined via Eq. (12), and plotted against the experimental data, as shown in Fig. 11. Based on the comparison presented in Fig. 11, it is found that the predicted results are in good agreement with the experimental lives and the data fall within the factor 2 bound. In contrast to the comparison shown in Fig. 8, based on the cumulative plastic strain energy approach, it reveals that an accurate description of the shape of stable hysteresis loop would lead to a satisfactory fatigue life prediction.

In this study, in order to realize which of those used life curves provides the best prediction performance, the following format is applied:

$$\Omega = \sqrt{\sum_{i=1}^{n} \frac{(\Delta_i - \Delta'')^2}{n-1}} \tag{13}$$

where Δ_i represents the ratio of the predicted result to the experimental value, and Δ'' is the average value of all calculated Δ_i. In Eq. (13), the value for n is the total number of data. Based on the data presented on Figs. 9-11, the calculated results for Ω are presented in Table 3. According the calculated results presented in Table 4, it is found that the value for Ω due to the $\varepsilon_a\sigma_{max}$-based life curve expressed as a power law function is minimum. The observation indicates that the relationship between $\varepsilon_a\sigma_{max}$ and $2N_f$ expressed as a power-low relationship provides the best prediction performance in this study. Moreover, for the case of data presented in Fig. 9, the calculated value for Ω based on the power-law relationship is less than that of the Basquin-Coffin-Manson relationship. Therefore, the power-law relationship provides better life prediction than the Basquin-Coffin-Manson relationship.

V. CONCLUSIONS

This paper has presented an experimental investigation into

the monotonic and cyclic deformation behavior of AISI 316 stainless steel. The monotonic stress-strain curve, cyclic stress-strain curve, the shape of stable hysteresis loop are simulated and the fatigue life curves based on the damage parameters ε_a, $\sigma_{\max}\varepsilon_a$ and W_f are developed. Based on the experimental observations and the comparison between the experimental and simulated results, the following conclusions are drawn:

1. At all applied strain amplitudes, it is observed that the variation of the measured stress amplitude per cycle with cycle presents a rapid increase at initially about ten cycles, then the stress response per cycle gradually decreases prior to failure.
2. The tested AISI 316 stainless steel is a cyclic hardening material via the comparison between the monotonic and cyclic stress-strain curves.
3. According the compassion between the Massing cyclic stress-strain behavior and eight actual hysteresis loops plotted in relation coordinates, the fact is observed that the Massing cyclic stress-strain behavior is absent in the tested AISI 316 stainless steel.
4. For the absence of Massing cyclic stress-strain behavior, based on the Ramberg-Osgood type Equation, the shape of hysteresis loop is modeled and obtained well simulated results with the aid of the Massing stress-strain curve and the well fitted ΔW_p - $\Delta\varepsilon$ curve.
5. For the tested AISI 316 stainless steel, the power-law relationship for the life curves based on the damage parameters ε_a and $\sigma_{\max}\varepsilon_a$ is a viable and valid expression.
6. Based on the observation in Fig. 11, the predicted values of the damage parameter W_f calculated on the basis of the simulated hysteresis loop provide reasonably good life predictions when compared with experimental lives.

REFERENCES

Abduluyahed, A. A. and K. J. Kurzydlowski (1998). Tensile properties of a type 316 stainless steel in air and vacuum. Materials Science and Engineering A 256, 34-38.

Bower, A. F. (1989). Cyclic hardening properties of hard-drawn copper and rail steel. Journal of the Mechanics and Physics of Solids 37, 455-470.

Bacon, D. H., L. Edwards, J. E. Moffatt and, M. E. Fitzpatrick (2013). Fatigue and fracture of a 316 stainless steel metal matrix composite reinforced with 25% titanium diboride. International Journal of Fatigue 48, 39-47.

Chaboche, J. L. (1991). On some modifications of kinematic hardening to improve the description of ratcheting effects. International Journal of Plasticity 7, 661-678.

Garud, Y. S. (1981). A new approach to the evaluation of fatigue under multiaxial loading. Journal of Engineering Material Technology 103, 118-125.

Halford G. R. (1966). The energy required for fatigue. Journal of Materials 1, 3-18.

Kwofie, S. (2003). Description of cyclic hysteresis behavior based on parameter model", Materials Science and Engineering A 357, 86-93.

Kamaya, M. (2010). Fatigue properties of 316 stainless steel and its failure due to internal cracks in low-cycle and extremely low-cycle fatigue regimes. International Journal of Fatigue 32, 1081-1089.

Lefebvre, D. and F. Ellyin (1984). Cyclic response and Inelastic Strain Energy in Low Cycle Fatigue. International Journal of Fatigue 26, 9-15.

Morrow J. D. (1965). Internal friction, damping and cyclic plasticity, ASTM STP 378, American Society for Testing and Material, Philadelphia, 45-87.

Mroz, Z. (1967). On the description of anisotropic work hardening. Journal of the Mechanics and Physics of Solids 15, 163-175.

Prager, W. (1956). A new method of analyzing stresses and strains in work hardening plastic solids. Journal of Applied Mechanics 23, 493-496.

Polak, J., F. Fardoun and S. Degallaix (1996). Effective and internal stress in cyclic straining of 316 stainless steel. Materials Science and Engineering A 215, 104-112.

Paiva, O. C. and M. A. Barbosa (2008). Microstructure, mechanical properties and chemical degradation of brazed AISI 316 stainless steel/alumina systems. Materials Science and Engineering A 480, 306-315.

Smith, K. N., P. Watson and T. H. Topper (1970). A Stress-Strain Function for the Fatigue of Metals. Journal of Material 5, 767-778.

Tokaji, K., K. Kohyama and M. Akita (2004). Fatigue behaviour and fracture mechanism of a 316 stainless steel hardened by carburizing. International Journal of Fatigue 26, 543-551.

Valanis, K. C. (1980). Fundamental Consequence of a New Intrinsic Time Measure-Plasticity as a Limit of the Endochronic Theory. Archives of Mechanics 32, 171-191.

Wittke, H. and K.-T. Rie (1998). Phenomenological and physically based on description of the deformation behavior in cyclic plasticity. Materials Science and Engineering A 247, 195-203.

Wang, X.-L., Y. D. Wang, A. D. Stoica, D. J. Horton, H. Tian, P. K. Liaw, H. Choo, J. W. Richardson and E. Maxey (2005). Inter- and intragranular stresses in cyclically-deformed 316 stainless steel. Materials Science and Engineering A 399, 114-119.